Transitions in Discrete Absorption Bands of Au_{130} Clusters upon Stepwise Charging by Spectroelectrochemistry

Dengchao Wang, Jonathan W. Padelford, Tarushee Ahuja, and Gangli Wang*

Department of Chemistry, Georgia State University, Atlanta, Georgia 30302, United States

ABSTRACT

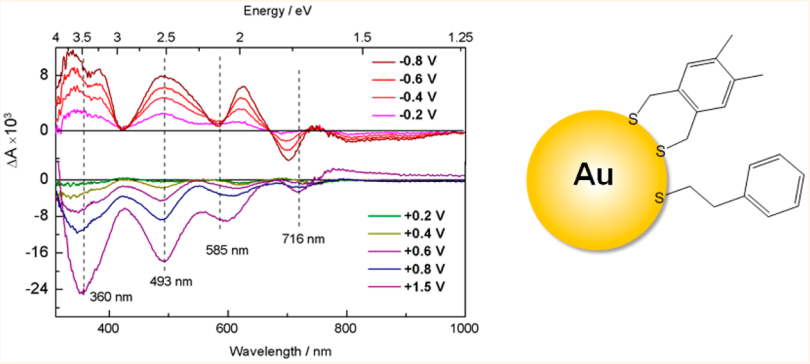

Rich and tunable physicochemical properties make noble metal clusters promising candidates as novel nanomolecules for a variety of applications. Spectroelectrochemistry analysis is employed to resolve previously inaccessible electronic transitions in Au_{130} clusters stabilized by a monolayer of di- and monothiolate ligands. Well-defined quantized double-layer charging of the Au core and oxidizable ligands make this Au_{130} nanocluster unique among others and enable selective electrolysis to different core and ligand charge states. Subsequent analysis of the corresponding absorption changes reveals that different absorption bands originate from different electronic transitions involving both metal core energy states and ligand molecular orbitals. Besides the four discrete absorption bands in the steady-state UV—visible—near-IR absorption spectrum, additional transitions otherwise not detectable are resolved upon selective addition/removal of electrons at cores and ligand energy states, respectively, upon electrolysis. An energy diagram is proposed that successfully explains the major features observed in electrochemistry and absorption spectroscopy. Those assignments are believed applicable and effective to explain similar transitions observed in some other Au thiolate clusters.

KEYWORDS: gold clusters · Au MPCs · Au_{130} · spectroelectrochemistry · electronic structures · energy diagram

Significant progress has been achieved recently to establish noble metal clusters as new types of functional nanomolecules with known molecular compositions and atomic structures.[1,2] Their rich optical, electrochemical, magnetic, and other physicochemical properties[3−5] make the metal clusters promising candidates for biomedical science, sensing, nanoelectronics, catalysis, and other energy technologies.[6−8] To control and tune those properties for broader and more effective applications, there are fundamental questions to be answered.[7]

Evidences accumulate that the size, structure, and charge states of the Au core, as well as Au—S interface bonding (*i.e.*, S—Au—S staple motif), collectively determine the energetic structures and related properties of monolayer-protected Au clusters (Au MPCs).[9−12] One of the key questions is that the respective contribution of those factors and the physical origin of many electronic transitions, particularly those related to excited states *via* photo- or electrochemical stimulation, remain to be elucidated. An extensively studied cluster is Au_{25}, in which the magnetism, catalytic activity, photoluminescence efficiency, and other physicochemical properties are found to be highly dependent on the charges on the Au core as well as the type of ligands

* Address correspondence to glwang@gsu.edu.

Received for review May 18, 2015 and accepted July 13, 2015.

Published online July 13, 2015
10.1021/acsnano.5b03007

© 2015 American Chemical Society

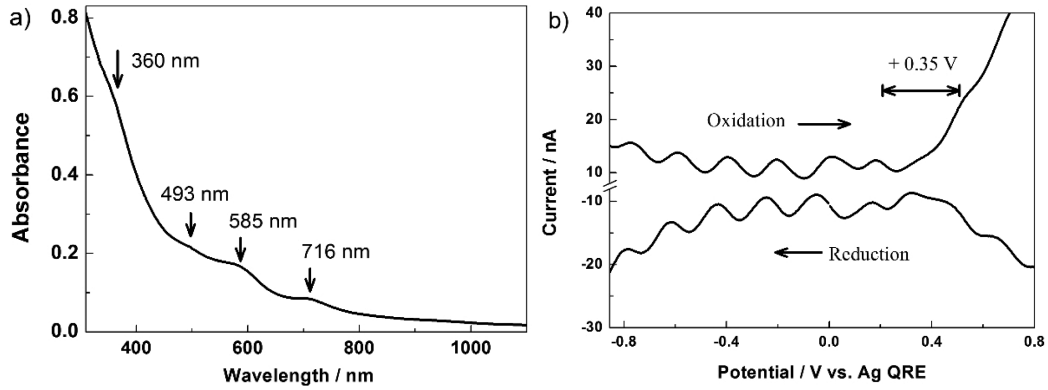

Figure 1. (a) UV−vis absorption spectrum and (b) differential pulse voltammograms (DPVs) of the Au_{130} nanoclusters in CH_2Cl_2.

used.[13−18] Systematic studies on other cluster systems would offer much needed insights to establish predictive models for the development of materials with desired properties for target applications.

At the transition size range from small molecules to plasmonic Au nanoparticles, discrete absorption transitions or intensity decays with less distinct features can be observed in the UV−visible−near-infrared spectrum range from different Au clusters.[8] Electrochemically, quantized double-layer (QDL) charging and split HOMO−LUMO-type electron transfer (ET) behaviors have been observed from larger (*i.e.*, more than 100 Au atoms) and smaller (a few tens of Au atoms) clusters, respectively.[8] Electrogenerated chemiluminescence (ECL) has been reported recently, enriching the electrochemical and optical activities of these Au clusters.[19,20] Once photoexcited, the Au clusters display broad and intense near-IR photoluminescence (*i.e.*, 650−1000 nm) with long lifetimes (up to microseconds), suggesting an energy relaxation process.[21] While atomic orbitals from Au(d), Au(sp), and S(p) have been employed to explain some optical and electrochemical features,[12,22] the respective contributions of Au, S, and the remaining ligand molecular orbitals to individual optical and electrochemical transitions remain to be established for various clusters. Further, because the remaining portion of the ligands, other than sulfur atoms that bind to Au as considered in most cases, is mostly inert in earlier studies, whether the molecular orbitals of the ligands (if adopted and within the energy range) could interact with or affect the electronic transitions of Au clusters remains to be established experimentally.[8,23]

Spectroelectrochemistry combines the merits of optical and electrochemical techniques: the core's and the ligands' redox states can be actively controlled *via* electrochemistry; the absorbance at different charge states can be recorded after electrolysis; the energy states of those corresponding electronic transitions can be correlated accordingly.[24,25] This report studies a large Au_{130} cluster with some ligands that can be electrochemically activated.[26] Spectroelectrochemistry is shown as a readily accessible technique to conveniently provide new fundamental insights for metal clusters. Such knowledge in the literature remains scarce and is mainly obtained by ultrafast transient absorption spectroscopy.[27−29] The later tool offers lifetimes in addition to detailed electronic transitions but requires more advanced instrumentation and thus has less accessibility.

RESULTS AND DISSCUSION

The synthesis, purification, and characterization of $Au_{130}(Dur\text{-}DT)_{29}(PET)_{22}$ employed in this report follow a previous report in which Dur-DT and PET refer to durene-dithiolate and phenylethanethiolate ligands, respectively.[26] Steady-state UV−visible absorption and voltammetry features are shown in Figure 1, which serve as reference points for the following spectroelectrochemistry analysis. Four discrete absorption bands around 360, 493, 585, and 716 nm are resolved (by first derivatives) from the absorption spectrum. Uniformly spaced QDL peaks (ΔE = 0.193 V) are separated by a 0.35 V gap toward more positive and negative potentials as shown in the differential pulse voltammograms (DPVs). The small gap is consistent with the earlier prediction of the transition from Au_{14x} (x varied from 0 to 7 in earlier literature) to Au_{130} size ranges.[8] Cyclic voltammograms at different scan rates and peak spacing analysis are included in Figure SI-1. The constant 59 mV potential difference between reduction and oxidation peaks in each pair of QDL peaks suggests facile and reversible core charging/discharging electron transfer activities. Therefore, the Au_{130} clusters at different core charge states have very good stability, allowing further spectroelectrochemical studies.

At higher potentials, ET activities involving thiolate ligands could occur. Irreversible ET processes accessing ligand and Au(x)-ligand orbitals are observed in the cyclic voltammograms (CVs) at a wider potential window shown in Figure SI-2.[26] Specific to the durene-dithiolate ligands, a prominent oxidation peak at *ca.* +1.32 V and a reduction at *ca.* −2.06 V are found for the

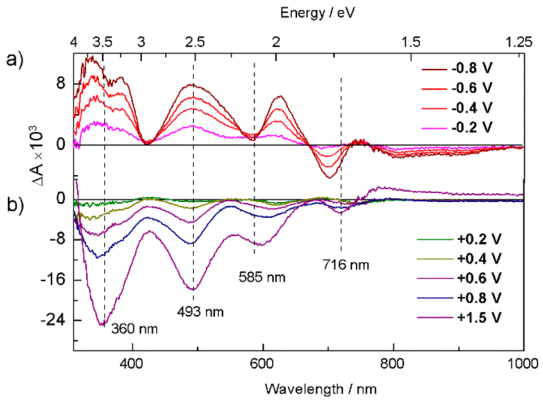

Figure 2. Differential absorption spectra under different bias potentials: (a) reduction- and (b) oxidation-induced transitions. The top (eV) and bottom (nm) axes directly correlate the spectrum features with the energy diagram.

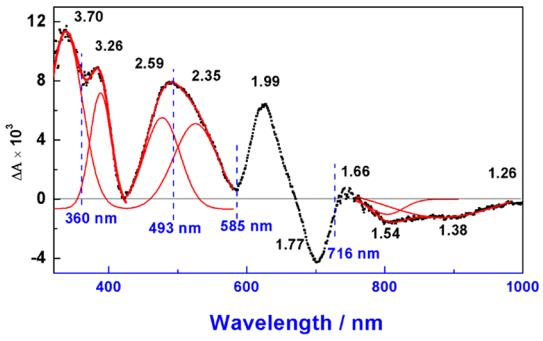

Figure 3. Gaussian fittings (dash lines) for the 360 and 493 nm band in the differential absorption curve at −0.8 V. Four peaks with positive ΔA centered at 335, 380, 478, and 526 nm and two peaks with negative ΔA around 805 and 900 nm are deconvoluted.

Au_{130} clusters. The CVs from a 2:1 Au/Dur-DT complex and a 1:1 Au/Dur-DT complex are also provided for comparison. These complexes, known to be oligo/polymeric mixtures in general as intermediates when synthesizing Au clusters, could be perceived as Au(I)ish and as Au(II)ish, respectively, considering each Dur-DT has two −SH groups and their possible bond motifs on Au core surfaces as ligands.[11] The ET potentials (peak or half-wave $E_{1/2}$) of thiolate ligands on a nanosized gold core, such as oxidative and reductive desorption, are slightly shifted from those observed from the Au(X) complexes and those on a flat Au surface, *i.e.*, self-assembled monolayer that has been widely studied.[30]

The spectroelectrochemistry setup is illustrated in Scheme SI-1. Briefly, a three-electrode electrochemical cell was built in an asymmetric quartz cuvette (0.1 × 1 cm). A large Pt mesh was used as a working electrode in the light path (0.1 cm). A Pt foil as the counter electrode and an Ag wire as the quasi-reference electrode (QRE) were positioned away from the light path. The thin layer and relative low sample concentration enable fast electrolysis within minutes. The majority of Au_{130} clusters in the light path can be charged to the desired charge states, monitored by the current decay to *ca.* 10% of initial value at a given potential. An absorption spectrum is recorded after each electrolysis. Due to the ligand oxidation process being irreversible, the absorbance spectra under +1.5 V (Dur-DT ligand oxidation) are taken after 1−2 min of electrolysis.

Differential absorption spectra in Figure 2 were obtained by subtracting the spectrum at 0 V from those recorded at different potentials, *i.e.*, different charge states after electrolysis. The original spectra are included in Figure SI-3. The four main peaks from the original sample are indicated by the dashed lines among those rich transitions newly resolved. Upon further reduction of the Au core (panel a), the absorption bands around 3.5, 2.5, and 2 eV intensify. A negative ΔA is observed showing a valley at 1.77 eV and a broad decrease from 1.66 eV to 1.26 eV. Interestingly, the 585 nm peak is one of the zones (another two around 2.90 and 1.66 eV) that remain largely unchanged. A well-defined isosbestic point at 1.85 eV suggests the conversion between the 1.99 eV peak and the 1.77 eV valley (sum at 3.76 eV). In the core oxidation (+0.2 to +0.8 V) shown in panel b, the intensity at all four peaks decreases. A notable feature is the shift in the peak position from *ca.* 2 eV in the reduction panel toward the 585 nm band upon oxidation. In addition to those decreased bands, upon ligand oxidation at +1.5 V, the intensity increases broadly below 1.66 eV.

The spectra after reduction electrolysis clearly display two components in the 360 and 493 nm absorption bands. Gaussian fittings of the differential spectrum at −0.8 V are shown in Figure 3. The 360 nm band is deconvoluted into two peaks centered at 335 and 380 nm (3.70 and 3.26 eV), while the 493 nm band is deconvoluted into 478 and 526 nm (2.59 and 2.35 eV). It appears that the 3.26 eV peak remains in position while the 3.70 eV peak shifts toward the 360 nm band when further oxidized. While the plasmonic band for few-nanometer Au nanoparticles (at 520 nm, 2.38 eV) is not discernible for most Au clusters, it is intriguing to observe the emergence of a 2.35 eV band upon reduction.

Before an energy diagram is proposed to attribute the corresponding transitions, an important concept about the electrochemical features at different charge states is explained in Figure 4. After each electrolysis, the majority of clusters in the bulk solution have been converted into the products of the corresponding ET reactions. It is obvious that the QDL peaks, still with uniform peak spacing in each voltammogram, are stretched or compressed upon the charging to the respective potentials as shown in panel a. Extra charges on the Au core will require counterions to maintain charge neutrality in solution. Both core charges (at the core−ligand interface beneath the ligand monolayer) and counterion penetration (into the monolayer from outside) are known to decrease the capacitance, which

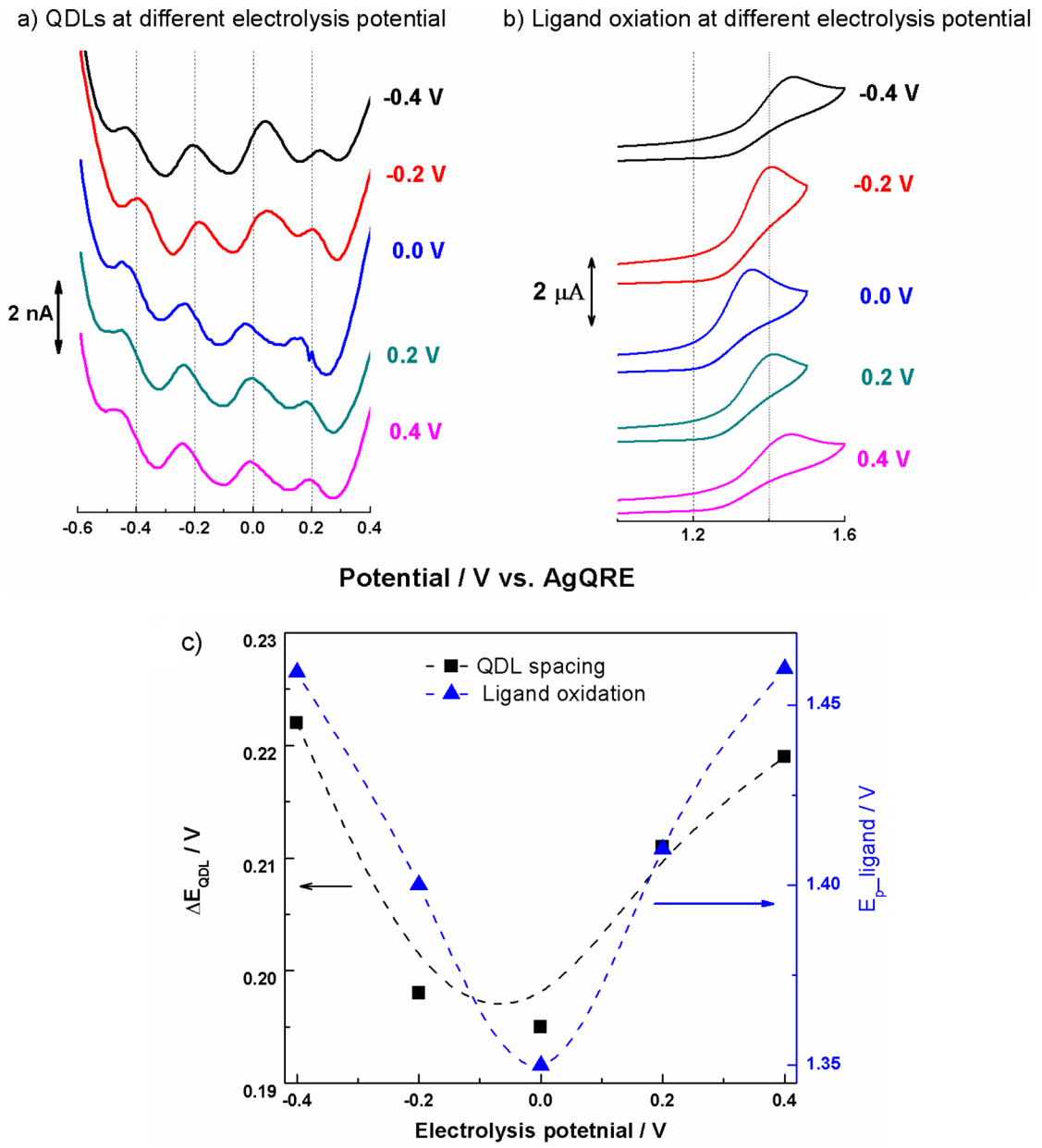

Figure 4. (a) QDL peaks resolved from the DPVs; (b) irreversible ligand oxidation from the CVs; and (c) data analysis after bulk electrolysis at different potentials (or different core charge states). Dash lines in panel c are added to show the trend (not fitting).

leads to the increase in charging energy, *i.e.*, peak spacing ΔE.[31] Accordingly, the ligand oxidation potential is also shifted as shown in panel b. This change in QDL peak spacing, though small at the *ca.* 10 mV range as analyzed in panel c (similar trends shown in Figure SI-4 from another sample with smaller changes), indicates the coupling between the core and peripheral charges (or dipoles). The QDL peak spacing at each electrolysis potential is the averaged peak−peak distances of all the peaks shown in each curve. Because the changes induced by one electron charging (*i.e.*, from 0 to −0.2 V) is small, a total or the averaged value presented herein offers a better signal/noise ratio. Small variations of individual peak spacing in each curve might indicate splitting and shifting in the degeneracy of those energy states upon charging that will require better S/N in further studies. Such interaction at the core−ligand interface is expected to be dynamic, which adds complexity reflected in the proposed energy diagram.

The energy diagrams of the native Au_{130} clusters and those after reduction are proposed in Figure 5. Those energy states involved in the distinct absorption transitions are sketched. The diagram of the oxidized form is relatively straightforward to explain and thus not plotted separately. The open-circuit potential (or rest potential) is slightly positive for as-synthesized Au_{130} clusters, *i.e.*, +0.18 V for this sample, which is used to

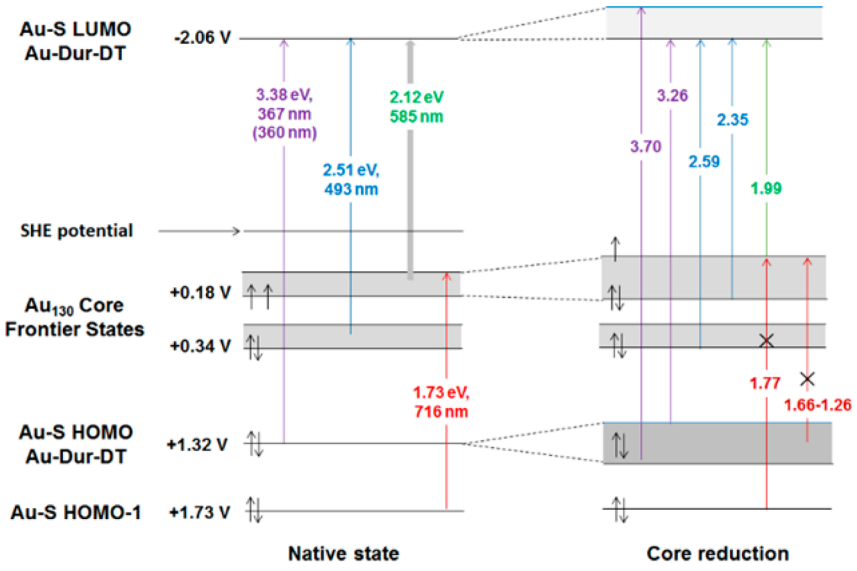

Figure 5. Proposed energy diagram for the Au_{130} nanoclusters at native and reduction states. Some involved energy states would be split and shifted when the core is reduced. The arrows indicate the transferred electrons during the core oxidation/reduction processes. All the potential values are measured with respect to AgQRE (+0.22 V *vs* SHE). The SHE potential is indicated in the diagram at −0.22 V.

define the core frontier states. The 0.35 V gap after two-electron oxidation from 0 V (Figure 1) suggests that there is an energy state immediately below the core frontier states (0.35 − ΔE + 0.18 = 0.34 eV, ΔE is the charging energy, 0.19 V). In consideration of the one-charge difference of the Au clusters in the diffuse layer after ET reactions and possible heterogeneity of the Au clusters (both charge states and composition), ΔE is added into these two states as possible band boundaries (error bar).

At +1.32 and −2.06 V (Figure SI-2), ET activities reveal the Au-Dur-DT HOMO and LUMO states. For monothiolate Au clusters, the Au atom in the staple motif (RS-Au-SR) is slightly more positive than Au(I) complexes. Because the bond structures of the dithiolate Dur-DT on Au clusters are currently unknown although inner Au core structures are determined,[32] the corresponding redox potentials of the two Au-Dur-DT complexes are employed to define the range of the HOMO and LUMO states, respectively. Absorption transitions to the Au-Dur-DT LUMO could therefore involve the −2.06 V states observed from the Au_{130} clusters and possibly −2.20 and −2.39 V ones at different time scale that will require transient absorption measurements beyond the scope of this report. It is important to emphasize that due to the chemically irreversible desorption of thiolates, the listed potential values ($E_{1/2}$) could involve several processes spanning over a potential range rather than a specific value. A weak oxidation band at around +0.9 V can be resolved as previously reported.[33] The transition from this state to higher energy states, *i.e.*, core frontier states, could not be detected with the spectrometer employed. This state is not included in the diagram for clarity. The oxidation peak around +1.73 V (Figure SI-5) is denoted as Au−S HOMO−1, from either the Au−PET bonding or one of the two sulfurs on Dur-DT that bonds to Au similar to the monothiols, or both.

For the as-synthesized Au clusters, *i.e.*, native state on the left, all four main absorption bands can be assigned with the transitions among these energy states very well. The 360 nm (3.44 eV) band is also observed from the two Au-Dur-DT complexes (Figure SI-6) and thus arises from the Au-Dur-DT HOMO−LUMO transitions. The minor difference from the electrochemistry states (1.32 + 2.06 = 3.38 *vs* 3.44) is attributed to the broad potential range, particularly from the chemically irreversible reduction process. Considering the reduction of the two complexes at −2.20 and −2.39 V, respectively, a *ca.* −2.12 V state in the midst of this broad band would give almost perfect assignment. Similarly, the 493 (2.51 eV) and 585 nm (2.12 eV) bands are attributed to the transitions from the core frontier states to the Au-Dur-DT LUMO. The transition from the Au−S HOMO−1 state to the partially filled core frontier states leads to the weak band around 716 nm (1.73 eV). This assignment also explains and is supported by the weak band observed around 700 nm from different Au_{130}−Au_{144} clusters.[34−36] The minor peak shift reflects the differences in the core energy states of those clusters presumably. The transitions from the Au-Dur-DT HOMO to core frontier states would constitute the diminishing yet-nonzero absorbance extending beyond the detection range (1100 nm). Furthermore, transition from the +0.34 V states to the upper edge of the frontier states would generate the expected optical gap that could not be directly measured herein.

Oxidation or reduction processes will change the electron density of the Au clusters. Charge-dependent changes in UV−visible absorption peaks have been

observed from $Au_{25}(PET)_{18}$ through homogeneous electron transfer reactions. At higher cluster charge states, the discrete absorption peaks become better defined with increased intensity.[15] The excess electrons or holes are expected to reside/delocalize at the core−ligand interface. The splitting and shifting of the peak wavelength reveal the corresponding shifted or split energy states at the interfacial Au−S bonding. The rationale further validates the proposed energy diagram retrospectively elaborated next.

In the reduction diagram, additional electrons in the core frontier states will inhibit the excitation from the lower states, which explains the broad decrease at the 1.66 to 1.26 eV range (rightmost arrow). Consequently, the excitation to the Au-Dur-DT LUMO state will intensify. Further, the excess electrons are speculated to shift the density of states corresponding to Au (II)ish toward Au(I)ish type bonding at the core−ligand interface (*i.e.*, the −2.20 V one from the Au(II)ish complex in Figure SI-2). Using the −2.06 and −2.39 V as boundaries, the 3.70 and 3.26 eV transitions are aligned almost perfectly. The argument requires finite structure information on the core−ligand bonding that is not available currently. Time-resolved transitions could reveal the corresponding time constant that is not accessible in this study. The excess electrons appear to change the degeneracy of the frontier states and lift the upper edge slightly. This is attested by the well-defined isosbestic point at 1.85 eV that separates the new 1.99 eV peak and the 1.77 eV valley (a total of 3.76 eV that matches the Au−S HOMO to LUMO transitions!). It is worth mentioning that both transitions are observed in the differential spectrum only by spectroelectrochemistry. The two areas match each other well, which strongly suggests the conversion between an enhancement and an inhibition of the respective transitions. Similarly, those additional electrons in the listed core states account for the enhancement and peak splitting of the 493 nm band. Other possible transitions between those states are not elaborated one by one, as they either remain unchanged or less changed compared to non-electrolyzed samples (*i.e.*, 585 nm band) or do not generate detectable signals (beyond the detection range).

The lower electron density upon further oxidation causes the decrease of all four absorption bands in general. It is obvious that the 493 and 585 nm band will decrease due to the lower electron density. One likely cause for the 360 nm band decrease is strong coupling of the core energy states and the ligand orbitals at the core−ligand bonding. The newly created holes would reside at the Au−S interface and thus lower all corresponding transitions. Besides the decrease in intensity, the very important observation supporting the proposed diagram is the blue shift of the ($-\Delta A$) valley at 1.99 eV toward the 585 nm absorption band and the corresponding red shift of the 1.77 eV (700 nm) valley toward the 716 nm absorption band. It is unknown if the absorbance at lower energy range, *i.e.*, from +1.32 to +0.18 = 1.14 eV, would increase with more states accessible limited by the spectrometer detection range. On the basis of our earlier studies, electrons in the core energy states could relax into those emptied ligand orbitals after the cation radical formation upon ligand oxidation at +1.5 V.[33] Accordingly, the new feature in the +1.5 V oxidation spectrum, albeit incomplete electrolysis and non-steady-state, reveals a broad increase below 1.66 eV. The observation not just further proves the earlier concept in the coupling of electrons in core states and Au−S ligand orbitals but also justifies the inclusion of broad Au-Dur-DT energy states illustrated in the reduction panel corresponding to the 1.66−1.26 eV transitions.

A definitive assignment of the hybridization of the corresponding atomic orbitals will require future theoretical analysis, *i.e.*, by density functional theory calculations. A qualitative understanding can be inferred from the extensively studied Au_{25} nanoclusters among many others in the literature.[11,12] Each energy state (Kohn−Sham) of a Au cluster is a hybridization of atomic orbitals including Au(5d), Au(6sp), S(3p), and others (often unspecified).[37] The Au core frontier states are likely composed predominantly of the sp bands of inner Au atoms, a rationale based on an inner Au_{13} core contributing almost exclusively to the HOMO−LUMO orbitals in Au_{25} clusters. Unlike PET or other inert ligands, in which the contributions of non-Au/S atoms are often perceived insignificant, additional molecular orbitals from Dur-DT ligands are accessible and constitute an increased portion of "others" at the respective energy states. The argument can be supported by the less recognized discussion on Au_{25} clusters, in which the electron donation from the $PhCH_2CH_2$ portion of the PET ligands has been employed to explain the red shift of the computed energy states compared to experiments.[37]

CONCLUSIONS

In summary, the Au_{130} nanoclusters electrolyzed to different charge states and the corresponding changes in optical absorption in the UV−visible−near-IR range are studied. New electronic transitions are resolved in the differential absorption spectrum by spectroelectrochemistry. Discrete absorption bands previously inaccessible are attributed to the transitions involving both core and ligand energy states. An energy diagram is established that successfully explains all major absorption features. The spectroelectrochemistry analysis and the atomic/molecular level energy diagram are believed to be applicable to other cluster systems to resolve the physical origins of different optical and electrochemical activities. With the establishment of a better resolved energy diagram, a new paradigm to

efficiently tune the electronic transitions in Au thiolate clusters can be achieved through the coupling/hybridization of appropriate ligand molecular orbitals with Au−S cluster energetics. Such capability is expected to enable better catalysis, bioimaging, and other applications.

EXPERIMENTAL SECTION

Au_{130} Synthesis and Purification. The preparation mainly followed previous reports. After the $HAuCl_4$ was phase transferred into toluene with tetraoctylammonium bromide (TOABr), 2-phenylethanethiol and durene-α_1,α_2-dithiol were added with stirring at a molar ratio of Au:PET:durene-DT = 1.5:2:1. The reaction mixture was stirred for 3 days after the reduction by $NaBH_4$. The final Au_{130} clusters were precipitated and washed by ample methanol and acetonitrile.

Electrochemistry. A CH Instruments 700c potentiostat was used to conduct the cyclic voltammetry and differential pulse voltammetry. Unless noted otherwise, a three-electrode system was used in all the electrochemistry tests comprising a 0.2 mm radius Pt disk electrode, a Pt foil as counter electrode, and an Ag wire as reference electrode. The Ag QRE potential was calibrated to be 0.22 V (*vs* SHE) by measuring the redox peak of ferrocenium/ferrocene (Fc^+/Fc) at 0.48 V. The solution was purged with argon gas for 15 min prior to the measurements.

Spectroelectrochemistry. A three-electrode electrochemical cell was built in a thin quartz cuvette. Bulk electrolysis was performed with a WaveNano potentiostat (Pine Instrument) using a large Pt mesh as working electrode, a Pt foil counter electrode, and a Ag wire quasi-reference electrode, as shown in Scheme SI-1. The concentration of the Au_{130} nanoclusters was around 10 μM, and 0.1 M tetrabutylammonium perchlorate was used as supporting electrolyte in CH_2Cl_2. The UV−vis absorption spectrum was recorded with a Shimadzu UV-1700 spectrophotometer.

Conflict of Interest: The authors declare no competing financial interest.

Supporting Information Available: Redox features of the free ligands, Au-Dur-DT complex, Au-PET complex, Au-PET plasmonic nanoclusters; charge state effect on the QDL spacing and ligand oxidation are included. The Supporting Information is available free of charge on the ACS Publications website at DOI: 10.1021/acsnano.5b03007.

Acknowledgment. The grant from the National Science Foundation (NSF CHE-1059022) is gratefully acknowledged. D.W. acknowledges the B&B fellowship from Georgia State University.

REFERENCES AND NOTES

1. Qian, H. F.; Zhu, M. Z.; Wu, Z. K.; Jin, R. C. Quantum Sized Gold Nanoclusters with Atomic Precision. *Acc. Chem. Res.* **2012**, *45*, 1470–1479.
2. Yang, H. Y.; Wang, Y.; Huang, H. Q.; Gell, L.; Lehtovaara, L.; Malola, S.; Hakkinen, H.; Zheng, N. F. All-Thiol-Stabilized Ag_{44} and $Au_{12}Ag_{32}$ Nanoparticles with Single-Crystal Structures. *Nat. Commun.* **2013**, *4*, 2422.
3. Alvarez, M. M.; Khoury, J. T.; Schaaff, T. G.; Shafigullin, M. N.; Vezmar, I.; Whetten, R. L. Optical Absorption Spectra of Nanocrystal Gold Molecules. *J. Phys. Chem. B* **1997**, *101*, 3706–3712.
4. Chen, S.; Ingram, R. S.; Hostetler, M. J.; Pietron, J. J.; Murray, R. W.; Schaaff, T. G.; Khoury, J. T.; Alvarez, M. M.; Whetten, R. L. Gold Nanoelectrodes of Varied Size: Transition to Molecule-Like Charging. *Science* **1998**, *280*, 2098–2101.
5. Zhu, M. Z.; Aikens, C. M.; Hendrich, M. P.; Gupta, R.; Qian, H. F.; Schatz, G. C.; Jin, R. C. Reversible Switching of Magnetism in Thiolate-Protected Au_{25} Superatoms. *J. Am. Chem. Soc.* **2009**, *131*, 2490–2492.
6. Zhou, C.; Yang, S. Y.; Liu, J. B.; Yu, M. X.; Zheng, J. Luminescent Gold Nanoparticles: A New Class of Nanoprobes for Biomedical Imaging. *Exp. Biol. Med.* **2013**, *238*, 1199–1209.
7. Li, G.; Jin, R. C. Atomically Precise Gold Nanoclusters as New Model Catalysts. *Acc. Chem. Res.* **2013**, *46*, 1749–1758.
8. Murray, R. W. Nanoelectrochemistry: Metal Nanoparticles, Nanoelectrodes, and Nanopores. *Chem. Rev.* **2008**, *108*, 2688–2720.
9. Jadzinsky, P. D.; Calero, G.; Ackerson, C. J.; Bushnell, D. A.; Kornberg, R. D. Structure of A Thiol Monolayer-Protected Gold Nanoparticle at 1.1 Å Resolution. *Science* **2007**, *318*, 430–433.
10. Tang, Z.; Xu, B.; Wu, B.; Germann, M. W.; Wang, G. Synthesis and Structural Determination of Multidentate 2,3-Dithiol-Stabilized Au Clusters. *J. Am. Chem. Soc.* **2010**, *132*, 3367–3374.
11. Hakkinen, H. The Gold-sulfur Interface at the Nanoscale. *Nat. Chem.* **2012**, *4*, 443–455.
12. Walter, M.; Akola, J.; Lopez-Acevedo, O.; Jadzinsky, P. D.; Calero, G.; Ackerson, C. J.; Whetten, R. L.; Gronbeck, H.; Hakkinen, H. A Unified Wiew of Ligand-Protected Gold Clusters as Superatom Complexes. *Proc. Natl. Acad. Sci. U. S. A.* **2008**, *105*, 9157–9162.
13. Antonello, S.; Hesari, M.; Polo, F.; Maran, F. Electron Transfer Catalysis with Monolayer Protected Au_{25} Clusters. *Nanoscale* **2012**, *4*, 5333–5342.
14. Zhu, Y.; Qian, H.; Drake, B.; Jin, R. Atomically Precise $Au_{25}(SR)_{18}$ Nanoparticles as Catalysts for the Selective Hydrogenation of Alpha, Beta-Unsaturated Ketones and Aldehydes. *Angew. Chem., Int. Ed.* **2010**, *49*, 1295–1298.
15. Wu, Z.; Jin, R. On the Ligand's Role in the Fluorescence of Gold Nanoclusters. *Nano Lett.* **2010**, *10*, 2568–2573.
16. Antonello, S.; Perera, N. V.; Ruzzi, M.; Gascon, J. A.; Maran, F. Interplay of Charge State, Lability, and Magnetism in the Molecule-Like $Au_{25}(SR)_{18}$ Cluster. *J. Am. Chem. Soc.* **2013**, *135*, 15585–15594.
17. Wang, G.; Huang, T.; Murray, R. W.; Menard, L.; Nuzzo, R. G. Near-IR Luminescence of Monolayer-Protected Metal Clusters. *J. Am. Chem. Soc.* **2005**, *127*, 812–813.
18. Wang, S.; Meng, X.; Das, A.; Li, T.; Song, Y.; Cao, T.; Zhu, X.; Zhu, M.; Jin, R. A 200-fold Quantum Yield Boost in the Photoluminescence of Silver-Doped Ag_xAu_{25-x} Nanoclusters: The 13 th Silver Atom Matters. *Angew. Chem., Int. Ed.* **2014**, *53*, 2376–2380.
19. Hesari, M.; Workentin, M. S.; Ding, Z. NIR Electrochemiluminescence from Au_{25} Nanoclusters Facilitated by Highly Oxidizing and Reducing Co-Reactant Radicals. *Chem. Sci.* **2014**, *5*, 3814–3822.
20. Hesari, M.; Ding, Z.; Workentin, M. S. Electrogenerated Chemiluminescence of Monodisperse $Au_{144}(SC_2H_4Ph)_{60}$ Clusters. *Organometallics* **2014**, *33*, 4888–4892.
21. Zheng, J.; Zhou, C.; Yu, M.; Liu, J. Different Sized Luminescent Gold Nanoparticles. *Nanoscale* **2012**, *4*, 4073–4083.
22. Link, S.; Beeby, A.; FitzGerald, S.; El-Sayed, M. A.; Schaaff, T. G.; Whetten, R. L. Visible to Infrared Luminescence from a 28-Atom Gold Cluster. *J. Phys. Chem. B* **2002**, *106*, 3410–3415.
23. Wolfe, R. L.; Balasubramanian, R.; Tracy, J. B.; Murray, R. W. Fully Ferrocenated Hexanethiolate Monolayer-Protected Gold Clusters. *Langmuir* **2007**, *23*, 2247–2254.
24. Ruiz, V.; Colina, A.; Heras, M. A.; López-Palacios, J. Potential Regulation of the Spectroelectrochemical Response of Monolayer-Protected Gold Cluster Films by Electrolyte Composition. *J. Phys. Chem. C* **2007**, *111*, 4277–4284.
25. Ung, T.; Giersig, M.; Dunstan, D.; Mulvaney, P. Spectroelectrochemistry of Colloidal Silver. *Langmuir* **1997**, *13*, 1773–1782.
26. Tang, Z.; Robinson, D. A.; Bokossa, N.; Xu, B.; Wang, S.; Wang, G. Mixed Dithiolate Durene-DT and Monothiolate

Phenylethanethiolate Protected Au_{130} Nanoparticles with Discrete Core and Core-Ligand Energy States. *J. Am. Chem. Soc.* **2011**, *133*, 16037–16044.
27. Yi, C.; Tofanelli, M. A.; Ackerson, C. J.; Knappenberger, K. L. Optical Properties and Electronic Energy Relaxation of Metallic $Au_{144}(SR)_{60}$ Nanoclusters. *J. Am. Chem. Soc.* **2013**, *135*, 18222–18228.
28. Green, T. D.; Knappenberger, K. L. Relaxation Dynamics of $Au_{25}L_{18}$ Nanoclusters Studied by Femtosecond Time-Resolved Near Infrared Transient Absorption Spectroscopy. *Nanoscale* **2012**, *4*, 4111–4118.
29. Stamplecoskie, K. G.; Kamat, P. V. Size-Dependent Excited State Behavior of Glutathione-Capped Gold Clusters and Their Light-Harvesting Capacity. *J. Am. Chem. Soc.* **2014**, *136*, 11093–11099.
30. Love, J. C.; Estroff, L. A.; Kriebel, J. K.; Nuzzo, R. G.; Whitesides, G. M. Self-Assembled Monolayers of Thiolates on Metals as A Form of Nanotechnology. *Chem. Rev.* **2005**, *105*, 1103–1170.
31. Laaksonen, T.; Ruiz, V.; Liljeroth, P.; Quinn, B. M. Quantised Charging of Monolayer-protected Nanoparticles. *Chem. Soc. Rev.* **2008**, *37*, 1836–1846.
32. Tlahuice-Flores, A.; Santiago, U.; Bahena, D.; Vinogradova, E.; Conroy, C. V.; Ahuja, T.; Bach, S. B. H.; Ponce, A.; Wang, G.; Jose-Yacaman, M.; Whetten, R. L. Structure of the Thiolated Au_{130} Cluster. *J. Phys. Chem. A* **2013**, *117*, 10470–10476.
33. Ahuja, T.; Wang, D.; Tang, Z.; Robinson, D.; Padelford, J.; Wang, G. Electronic Coupling between Ligand and Core Energy States in Dithiolate-Monothiolate Stabilized Au Clusters. *Phys. Chem. Chem. Phys.* **2015**, 10.1039/C5CP02685G.
34. Negishi, Y.; Sakamoto, C.; Ohyama, T.; Tsukuda, T. Synthesis and the Origin of the Stability of Thiolate-Protected Au_{130} and Au_{187} Clusters. *J. Phys. Chem. Lett.* **2012**, *3*, 1624–1628.
35. Qian, H. F.; Jin, R. C. Controlling Nanoparticles with Atomic Precision: The Case of $Au_{144}(SCH_2CH_2Ph)_{60}$. *Nano Lett.* **2009**, *9*, 4083–4087.
36. Jupally, V. R.; Dass, A. Synthesis of $Au_{130}(SR)_{50}$ and $Au_{130-x}Ag_x(SR)_{50}$ Nanomolecules through Core Size Conversion of Larger Metal Clusters. *Phys. Chem. Chem. Phys.* **2014**, *16*, 10473–10479.
37. Zhu, M.; Aikens, C. M.; Hollander, F. J.; Schatz, G. C.; Jin, R. Correlating the Crystal Structure of A Thiol-Protected Au_{25} Cluster and Optical Properties. *J. Am. Chem. Soc.* **2008**, *130*, 5883–5885.